Global trends in air-water CO_2 exchange over seagrass meadows revealed by atmospheric Eddy Covariance

[1]Bryce Van Dam, [2]Pierre Polsenaere, [3]Aylin Barreras-Apodaca, [4]Christian Lopes, [3]Zulia Sanchez-Mejia, [5,6]Tatsuki Tokoro, [6]Tomohiro Kuwae, [7]Lucia Gutiérrez Loza, [7]Anna Rutgersson

[1] Institute of Coastal Research, Helmholtz-Zentrum Geesthacht (HZG), Geesthacht, 21502, Germany

[2] IFREMER, Laboratoire Environnement et Ressources des Pertuis Charentais (LER-PC), BP133, 17390, La'Tremblade, France.

[3] Instituto Tecnológico de Sonora, Ciudad Obregón, Sonora, México

[4] Dept. of Biology and The Institute of Environment, Florida International University, 11200 SW 8th Street, Miami, FL 33199, USA

[5] Coastal and Estuarine Environment Research Group, Port and Airport Research Institute, Yokosuka, Japan

[6] National Institute for Environmental Studies, Center for Global Environmental Research (CGER), Office for Atmospheric and Oceanic Monitoring, Onogawa, Tsukuba, Ibaraki, Japan

[7] Department of Earth Sciences, Uppsala University, Uppsala, Sweden

Corresponding author: Bryce Van Dam, (Bryce.Dam@hzg.de)

Key Points:

- Direct measurements show that air-water CO_2 exchange over seagrass meadows is of similar magnitude to carbon burial rates
- Key drivers are tidal forcing, temperature, light, and wind, which trade off in importance over hourly-seasonal time scales
- Surface drag coefficients were greater than open water prediction, suggesting a near-universal gas transfer enhancement across all sites

Abstract

Coastal vegetated habitats like seagrass meadows can mitigate anthropogenic carbon emissions by sequestering CO_2 as "blue carbon" (BC). Already, some coastal ecosystems are actively managed to enhance BC storage, with associated BC stocks included in national greenhouse gas inventories or traded on international markets. However, the extent to which BC burial fluxes are enhanced or counteracted by other carbon fluxes, especially air-water CO_2 flux (FCO_2) remains poorly understood. To this end, we synthesized all available direct FCO_2 measurements over seagrass meadows made using a common method (atmospheric Eddy Covariance), across a globally-representative range of ecotypes. Of the four sites with seasonal data coverage, two were net CO_2 sources, with average FCO_2 equivalent to 44 - 115% of the global average BC burial rate. At the remaining sites, net CO_2 uptake was 101 - 888% of average BC burial. A wavelet coherence analysis demonstrates that FCO_2 was most strongly related to physical factors like temperature, wind, and tides. In particular, tidal forcing appears to shape global-scale patterns in FCO_2, likely due to a complex suite of drivers including: lateral carbon exchange, bottom-driven turbulence, and pore-water pumping. Lastly, sea-surface drag coefficients were always greater than prediction for the open ocean, supporting a universal enhancement of gas-transfer in shallow coastal waters. Our study points to the need for a more comprehensive approach to BC assessments, considering not only organic carbon storage, but also air-water CO_2 exchange, and its complex biogeochemical and physical drivers.

Plain Language Summary

Carbon storage is a valuable ecosystem service of seagrass meadows, serving as a possible pathway to draw down atmospheric carbon dioxide (CO_2) levels. However, this approach may be unsuccessful if carbon storage in sediments is exceeded by the release of CO_2 from the water. To better understand the scope of this problem, we compiled all available measurements of air-water CO_2 exchange over seagrass meadows. We found that rates of CO_2 release or uptake were indeed large, even when compared with potential rates of carbon storage in seagrass soils. However, these large air-water exchanges of CO_2 did not occur for the same reason everywhere. While light availability was sometimes a strong predictor of air-water CO_2 exchange, tidal mixing and temperature were also very important, revealing a much more complex network of drivers than previously thought. Despite these diverse conditions, we found one key similarity across all sites, in that rates of air-water gas transfer appear to always be greater than would be expected for the open ocean. Taken together, the results of our study show that assessments of carbon storage in coastal seagrass ecosystems will be incomplete if they do not consider exchanges of CO_2 between the water and air.

1. Introduction

The coastal ocean plays a disproportionately large role in global and regional carbon (C) cycles (Fennel et al., 2019; Friedlingstein et al., 2019; Laruelle et al., 2018). In particular, seagrass-inhabited regions receive large quantities of terrestrial and marine organic carbon, much of which is sequestered in sediments and stabilized by extensive root mats (Prentice et al., 2020; Röhr et al., 2018). Carbon fixed locally by seagrasses and their epiphytes is also buried here, constituting a net removal of C from the atmosphere (Duarte et al., 2005; Kennedy et al., 2010). Despite some uncertainty regarding its ultimate source, this 'blue carbon' reservoir (Macreadie et al., 2019; Kuwae and Hori 2019) is a globally significant, yet sensitive, carbon stock (Fourqurean et al., 2012). However, these relatively high C burial rates in seagrass meadows - reaching 0.22 g C m^{-2} yr^{-1} (Duarte et al,. 2005) - must also be considered in the context of other C flows through the ecosystem, which act synergistically or antagonistically to increase or decrease net C sequestration.

For example, the biotic or abiotic formation and burial of calcium carbonate in seagrass beds consumes alkalinity, thereby generating CO_2 (Burdige and Zimmerman 2002; Burdige et al., 2010; Hu and Burdige 2007). Likewise, the degradation of organic matter in anoxic sediments produces CH_4 and N_2O at rates that may affect the net global warming potential of seagrass meadows (Oreska et al., 2020). As a result, some seagrass beds, especially those receiving large loads of allochthonous organic matter (Al-Haj and Fulweiler 2020), or those where calcification rates are high (Howard et al., 2018), can be pushed towards net C source status, despite high rates of autotrophic C fixation (Macreadie et al., 2017). The extent to which calcification mitigates photosynthetic CO_2 uptake, pushing seagrass ecosystems towards CO_2 source status remains a hotly debated topic (Howard et al., 2018; Sanders et al., 2019). While it is suggested that CO_2 uptake is not affected by carbonate precipitation because carbonate minerals are largely imported from adjacent systems (Saderne et al., 2019), confirmation by direct CO_2 flux measurements does not yet exist.

Seagrass meadows may also vary between net ecosystem heterotrophy and autotrophy over daily to weekly time scales (Berg et al., 2019; Gazeau et al., 2005; Van Dam et al., 2019a). Elsewhere, the anaerobic generation of alkalinity, largely through sulfate reduction and burial (Dollar et al., 1991) and denitrification (Eyre and Ferguson 2002), can increase the buffering capacity of overlying water, enhancing atmospheric CO_2 uptake. Advection can also play a role, as seagrasses in river-dominated estuaries may receive waters over-saturated in CO_2, which is subsequently degassed in the wind-exposed coastal zone (Röhr et al., 2018). Regardless of the mechanism, it is clear that C sequestration in 'blue carbon' ecosystems is not simply the product of long-term organic carbon burial in sediments. Many other processes consume or produce dissolved inorganic carbon (DIC), such as calcification and anaerobic metabolism, thereby affecting air-water CO_2 fluxes (FCO_2), pushing these ecosystems towards net carbon sink or net source, independent of the organic carbon burial flux.

Given the broad global distribution of seagrasses, and the various coastal typologies they inhabit, it is no surprise that net ecosystem metabolism exhibits substantial geographic trends (Duarte et al., 2010). Likewise, FCO_2 in these systems is not uniform. In some regions, for example, light

limitation of photosynthesis may play a critical role in net ecosystem productivity (Berg et al., 2019; Long et al., 2015) and CO_2 uptake (Gazeau et al., 2005; Tokoro et al., 2014). Elsewhere, due to greater turbidity or water depth, this factor may carry little leverage, exceeded in importance by tides (Polsenaere et al., 2012) or water temperature (Van Dam et al., in review). Where temperature and biology allow, net ecosystem calcification may instead dominate water column carbonate chemistry (Perez et al., 2018; Van Dam et al., 2019a). These reasons and others may contribute to differences in FCO_2 for seagrass meadows located at comparable latitudes or in similar climates.

Rates of carbon burial can be reliably assessed using natural and anthropogenic radioactive tracers, integrating this process over a sufficiently long period as to accurately characterize burial over decadal to centurial scales. This is in stark contrast to FCO_2, where extreme temporal variability complicates attempts to integrate this flux over time. Existing 'bulk transfer' approaches to quantifying FCO_2 rely on discrete measurements of CO_2 partial pressure (pCO_2), which often miss out on high-frequency variability. These pCO_2 measurements are then combined with a gas transfer coefficient, the parameterization of which is notoriously challenging due to the diverse physical forcing of air-water gas exchange in shallow coastal waters (Borges et al., 2004). For these reasons, direct measurements of FCO_2 are desirable, relative to parameterized estimates. Atmospheric eddy-covariance (EC) has been used for decades to measure turbulent exchanges of gas and energy over terrestrial ecosystems (Aubinet et al., 2000; Baldocchi 2003), and the open ocean (Butterworth and Miller, 2016; Garbe et al., 2014; Wanninkhof et al., 2009). However, only recently has this approach begun to be used at nearshore intertidal or subtidal habitats (Chien et al., 2018; Honkanen et al., 2018; Ikawa et al., 2015; Rey-sánchez et al., 2017) including seagrass meadows (Polsenaere et al., 2012; Tokoro et al., 2014; Van Dam et al., in rev). Advantages of direct EC measurements of FCO_2 include: 1) continuous temporal coverage, 2) existence of standard methods for data processing, and 3) non-invasive and spatially representative measurements.

While direct FCO_2 measurements over seagrass meadows have existed for roughly a decade (Polsenaere et al., 2012), and some regional synthetic efforts have been made (Tokoro et al., 2014), these individual datasets have yet to be synthesized globally. Therefore, a set of very basic questions remains unanswered. Are there global patterns explaining why some seagrass meadows are CO_2 sinks and others are sources? Are these reasons typological, climatological, or simply latitudinal in nature? Are there any generalizable features of air-water CO_2 exchange across these diverse coastal habitats? These questions are central to 'blue carbon' science (Legge et al., 2020; Macreadie et al., 2019), but have yet to be addressed. In the present study, we synthesize a dataset of direct EC measurements of air-sea FCO_2 over seagrasses. While this dataset is limited to only sites in the Northern hemisphere, it is the most complete synthesis to date, representing a broad range in latitude and ecosystem characteristics. We describe global trends in FCO_2, discuss temporal and spatial variability and associated controls, and compare FCO_2 with literature estimates of carbon burial. A spectral decomposition is also used to identify sets of physical drivers important across temporal scales.

2. Materials and Methods

2.1. Study Sites

Direct EC measurements of FCO_2 were acquired for six subtidal or intertidal sites with seagrass coverage. Together, these sites represent a broad zonal (110° W to 145° E) and latitudinal (24° N to 57° N) range (Figure 1), and are described in table 1, along with the nearest recorded coastal typology from Dürr et al. (2011).

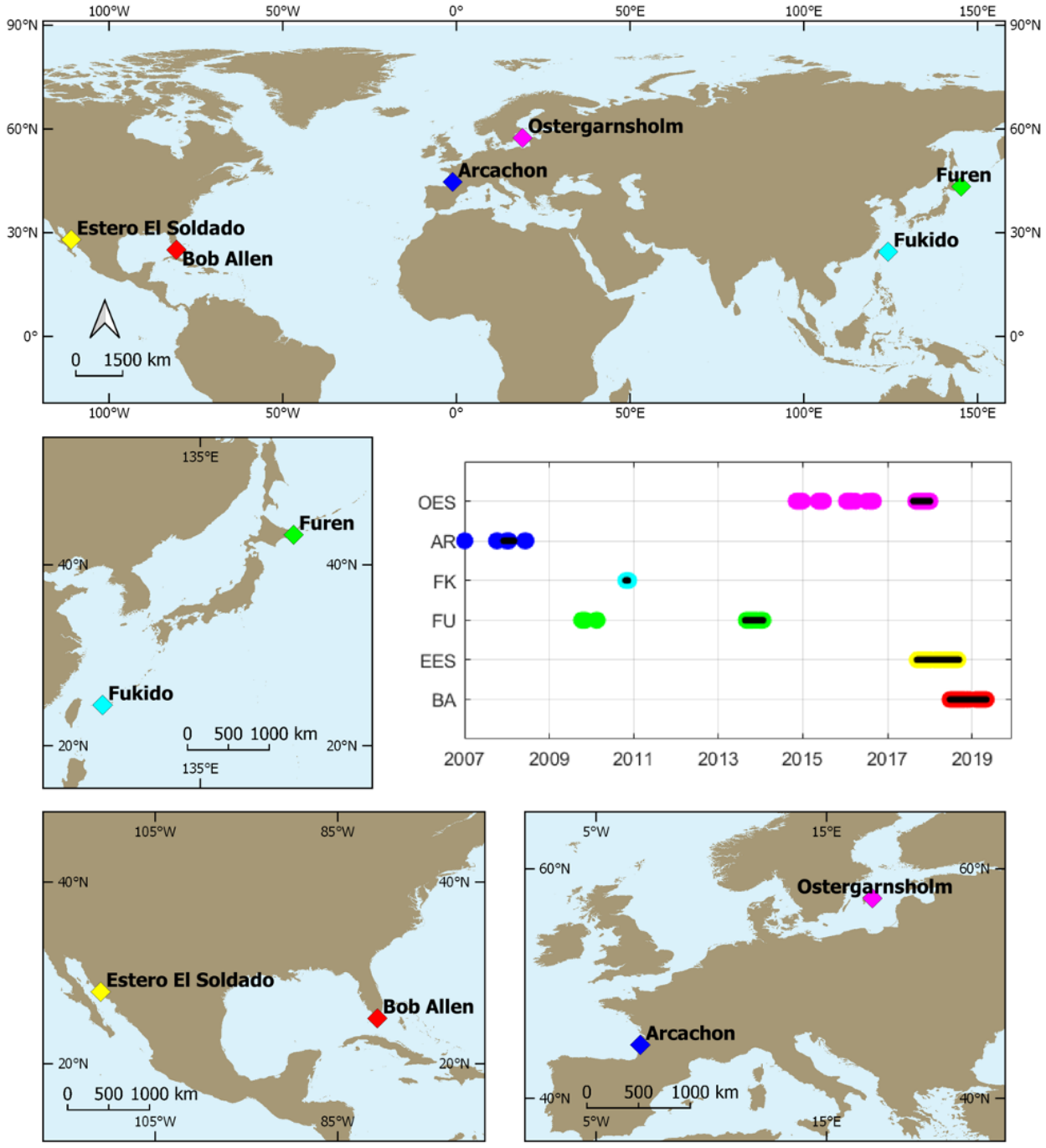

Figure 1. Site Maps, including inset figure of data coverage for each site, where the black bars indicate the subset of reasonably 'continuous' data used for the wavelet coherence analysis.

Site Name		Coastal Typology	Seagrass Community	Mean Daily Tidal Range (Tidal category)	Seagrass Biomass (gC or gDW m^{-2})	Lat-Long (decimal degree)	Days of data available (# Measurement Periods)	Methods Reference
Bob Allen Keys, USA	BA	Type VI (Karst)	*Thalassia testudinum*	0.048 m (small-tidal)	4.8 gC m^{-2}	25.03 -80.68	314 (1)	Van Dam et al. (2020)
Estero El Soldado, Mexico	EES	Type VII (Arheic)	*Zostera marina*	0.40 m (large-tidal•)	-	27.95 -110.97	357 (1)	Benítez-Valenzuela& Sanchez-Mejia 2020)
Furen lagoon, Japan	FU	Type I (Small Deltas)	*Zostera marina*	0.87 m (large-tidal)	16-318 g DW m^{-2}	43.33 145.26	146 (3)	Tokoro et al. (2014)
Fukido estuary, Japan	FK	Type I (Small Deltas)	*Cymodocea serrulata, Thalassia Hemprichii, Enhalus acoroides*	0.93 m (large-tidal)	32-88 g DW m^{-2}	24.49 124.23	25 (1)	Tokoro et al. (2014)
Arcachon Bay, France	AR	Type II (Tidal Systems)	*Zostera spp.*	1.8 m (large-tidal)	93.4 - 114.9 g DW m^{-2}	44.67 -1.67	530 (2)	Polsenaere et al. (2012)
Östergarnsholm, Sweden	OES	Type IV (Fjords or Fjaerds)	Unknown	<0.5 (small -tidal)	-	57.45 18.98	1,156 (1)	Lucía Gutiérrez-Loza et al. (2019)

Table 1. Summary table describing each site considered in this study, including the coastal typology (Dürr et al., 2011), and seagrass community and coverage statistics. Community and cover statistics are from Plus et al. (2010) and Carmen et al. (2019) for AR, from Tokoro et al. (2014) For FU and FK, from Armitage & Fourqurean (2011) for BA. Tidal ranges shown here were calculated from mean daily statistics over the entire study period, except for OES, where we apply a literature value of 0.5m (Sahlée et al., 2008). EES is considered a "large-tidal" site because it is located inside a tidal inlet where appreciable tidal currents exist despite a relatively low tidal range.

2.2. EC Measurements

While different analytical instruments were used at each site (Table 1), all EC measurements were conducted using coincident and rapid (10-20 Hz) measurements of CO_2 concentration and 3-D wind velocity. All EC systems relied on infrared gas analyzers (IRGA) produced by LI-COR Biosciences, USA. These IRGAs were either of an open- or closed-path configuration, depending on the environmental and power conditions at each site. Further information regarding the specific EC configurations used at each site can be found in the references shown in Table 1.

2.3. Data QA/QC

For all datasets processed using EddyPro software (Licor Biosciences, USA), data were screened to remove records with QC code (Burba 2010) greater than 1, resulting in a removal of 11.6% of the full dataset. Next, in an effort to screen out data where a terrestrial influence was likely, we removed results where the shear conditions indicated a non-marine flux footprint. As described later, we discarded FCO_2 results when the ratio of u_*/U_{mean} exceeded a threshold of 0.139, which was set as 150% of the average u_*/U_z (0.0924). This step resulted in the removal of an additional 14.6% of the data following QC code screening. Lastly, FCO_2 values greater than 3 standard deviations from the mean (FCO_2 > 10.4 µmol m^{-2} s^{-1}) were considered anomalous and were removed, representing a final 1.3% of the remaining dataset. Cumulatively, these screening steps removed 25.5% of the initial, post-processed dataset. In keeping with convention, negative FCO_2 indicates a net CO_2 uptake, while positive values represent CO_2 emission.

2.4. Energy balance

Energy balance assessments are important components of terrestrial EC studies, as these energy flows (radiative as well as latent and sensible heat exchanges) directly control local water budgets and hence many ecosystem processes. In an idealized system, inputs of energy net solar radiation (R_n) are exactly balanced by latent (i.e. evaporative) and sensible heat fluxes, LE and H respectively. Any departure from the 1:1 relationship between R_n and total heat loss (H+LE), suggests that EC measurements are missing some energy flux. This could be due to non-stationary conditions, when spatial gradients in a variable (i.e. temperature) are advected past the measurement site, causing, for example, LE+H to be greater/less than R_n. While these measurements may well be 'real', they can also be problematic because they indicate that factors outside the flux footprint have influenced the measured vertical fluxes at a given time. Likewise, energy can be stored in (or lost from) standing water when its temperature changes. In the present study, we have quantified this energy flux (J) and considered it in subsequent budget assessments. Because of the very high heat capacity of water, frequent departures from the 1:1 relationship between H+LE+J and R_n can be taken as indicators of lateral water exchange. This is of course concerning for EC studies of FCO_2 in shallow waters, where our goal is to attribute measured FCO_2 to processes happening inside the flux footprint (i.e. the seagrass meadow).

At sites where measurements of water temperature, water height, net solar radiation (R_n; W m^{-2}), latent heat flux (LE; W m^{-2}), and sensible heat flux (H; W m^{-2}) were available, it was possible to construct an approximate energy budget. We determine the closure of this energy balance as the difference between R_n and the sum of LE, H, and J, integrated over 24 hours (BA, EES, FK, OES) or 6 hours when water-side measurements were limited (AR). When R_n data were absent, R_n was estimated from photosynthetically active radiation (PAR; µmol photons m^{-2} s^{-1}) using an empirical relationship (R_n = -0.60 * PAR - 0.12; linear R^2 = 0.98) constructed using the combined dataset from this study.

The energy balance at OES is somewhat more challenging to assess, in part because of a relatively complex bathymetry, which makes it difficult to estimate the water depth over which the water-column energy storage (J) should be integrated. The presence of seasonal and periodic stratification, as well as greater absolute water depths (up to 40 m) further complicate the energy

balance here (Rutgersson et al., 2020). Therefore, for OES, we calculated J using a water depth of 5 m, which was the depth at which water temperature was measured.

2.5. Time-Frequency Analysis

A wavelet coherence analysis (Grinsted et al., 2004; Torrence and Compo 1998) was carried out to analyze the dependence of FCO_2 on net solar radiation (R_n), water depth (Z_{water}), air temperature (T_{air}), water temperature (T_{water}), wind speed (U_{mean}), and wind direction (U_{dir}). Due to the sporadic nature of these coastal EC deployments, the temporal coverage is somewhat patchy, creating a problem for time-series analysis. So, prior to wavelet coherence analysis, the largest period of contiguous data availability was identified for each site (black bars shown in Figure 1), and only this period was used for subsequent wavelet analysis. This necessary choice results in an improved data quality at hourly to monthly time scales, but necessarily involves a loss of information at longer scales. Gaps in the pseudo-continuous datasets for each site were filled with mean statistics for each variable, and the edges were padded with zeros. We forced each dataset into a normal distribution, applied a Morlet wavelet to the time series (Grinsted et al., 2004), and estimated the 95% confidence intervals with 15 Monte Carlo simulations.

3. Results and Discussion

3.1. Energy balance

The energy balance closure was best for BA, with daily average R_n closely balanced by net heat losses (H+LE+J) (Figures 2a, S1). This was not the case for the remaining sites for which a complete energy balance could be assessed (EES, FK, FU, AR, OES). At EES, most daily average heat losses (H+LE+J) fell below the 1:1 line (Figures 2b, S1), indicating either a measurement error, or the presence of a missing heat flux that we currently do not account for. At EES, this missing heat flux is plausibly related to horizontal advection and tidal exchange with the adjacent upwelling system. Similarly, low heat losses relative to R_n were observed at OES (Figure 3b), but the microtidal nature of this site suggests that the energy budget imbalance here could be related to horizontal advection and wind driven upwelling. The energy balance is further complicated at OES due to periodic stratification and variable water depths, and our approach of assuming a single, average water height to calculate J, may not be appropriate.

At FU, H+LE+J was always much less than R_n, indicating that water column heating was a major, yet unaccounted for, energy sink. In contrast to the previous sites where H+LE+J was typically less than R_n (EES, OES, FU), daily heat losses were always greater than R_n at both AR and FK (Figures 2c, 3a, S1). This suggests the presence of an additional heat source, beyond net solar radiation (R_n). Since tidal ranges are relatively large at both AR and FK, we suggest that tidal mixing was the source of warmer water, allowing heat losses through H and LE to exceed net solar inputs.

To further illustrate the role of tidal forcing on energy budgets, we calculate an energy balance residual (EBR) as ($EBR=[J+H+LE] - R_n$), which represents the departure from the 1:1 line in Figure S1. When EBR is plotted against the range in water height, it becomes clear that tidal forcing plays a key role in governing energy balances across a global distribution of seagrass

meadows (Figures 2 and 3). At both microtidal (BA) and tidal (EES and FK) sites, the intercept of EBR with tidal range is not significantly different from zero ($\alpha = 0.05$), indicating that the energy budget is in approximate closure when tidal forcing is not present. The y-intercept was not zero at FU (-374.7 ± 243.9 W m^{-2}), but the presence of a significant negative relationship between EBR and tidal range supports the role of tidal exchange as a sink for heat.

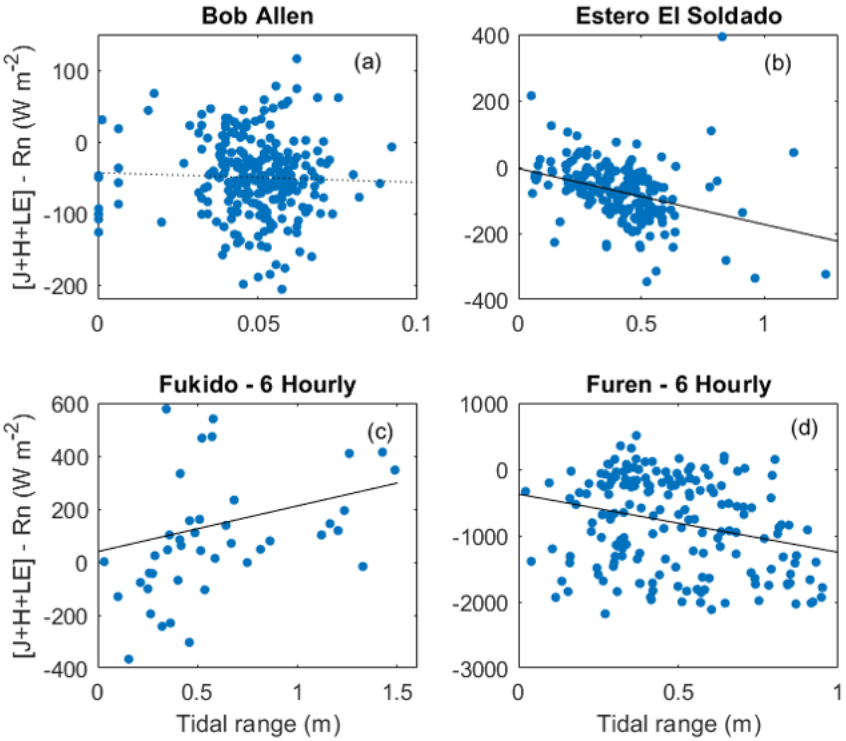

Figure 2. Energy balance residual EBR (difference between J+H+LE and R_n) versus tidal range for BA (a), EES (b), FK (c), and FU (d). Linear slopes for EES, FK, and FU are significantly different from zero and are shown in bold, while the slope is insignificant for BA (a).

At BA, there appears to be little energy 'leakage' due to tidal advection, as EBR does not vary with the daily range in water height (Figure 2a). However, at both tidal sites (EES and FK), there is a significant linear correlation between EBR and the tidal range ($\alpha = 0.05$). This relationship is positive for FK, such that energy inputs from R_n are exceeded by loss through LE, H, or J, with the difference increasing with tidal range (Figure 2c). This positive EBR implies an input of relatively warm water to the FK embayment, a likely event for a subtropical site during the summer (data for FK are from 23 July to 17 August 2011). The trend is reversed at EES, with EBR becoming more negative with increasing daily tidal range, implying a 'leakage' of energy via tidal exchange (Figure 2b). Because the seagrass meadows at EES are influenced by seasonal upwelling in the eastern Gulf of California (Lluch-Cota 2000), such a heat exchange between warm coastal waters and cooler, recently upwelled water appears plausible.

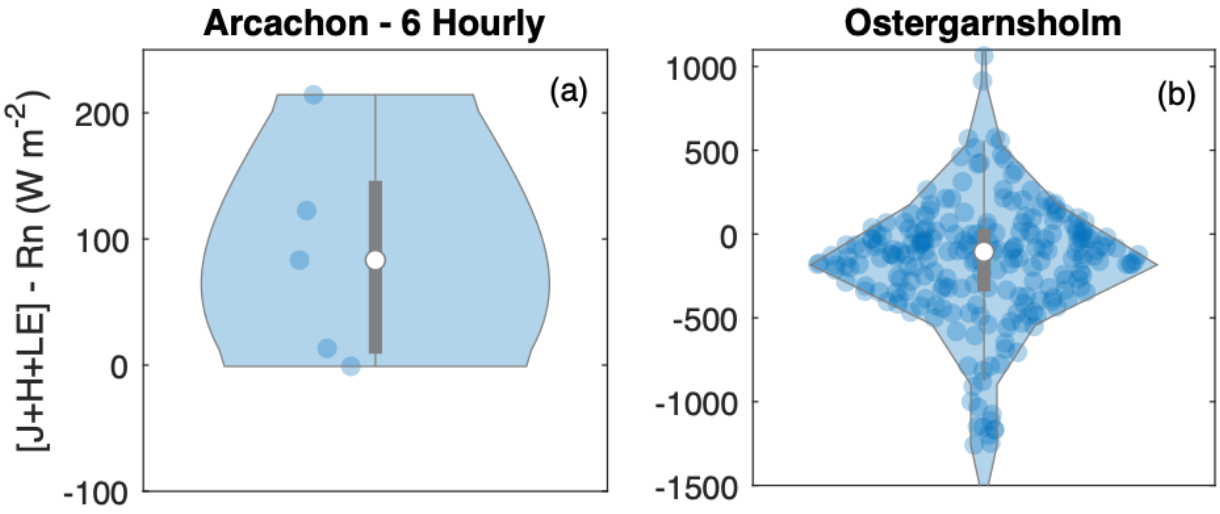

Figure 3. Violin plots of EBR for AR (a) and OES (b).

We used direct, EC measurements of heat fluxes as a conservative tracer, and showed that tidal forcing can explain large-scale trends in energy balances, despite some key site-specific differences. Because the subset of three sites considered here (BA, EES, FK) are at approximately the same latitude (Table 1), the impact of latitudinal differences in LE (Figure 6) can be excluded as a secondary factor. In subsequent sections, we will extend the results of this analysis to a non-conservative constituent, CO_2. We will discuss the impact of tidal mixing on air-water CO_2 exchange, in the context of the coastal 'blue carbon' sink.

3.2. General patterns and trends in FCO_2

FCO_2 was highly variable at all sites, fluctuating between sink (negative FCO_2) and source (positive) over the study period. Averaged over the entire study period, however, FCO_2 was negative for four sites (EES, FU, FK, AR) and positive for the other two sites (BA, OES). The spread of FCO_2 in micro-tidal regions (OES, BA) was much more narrow range than in tidal areas (FU, FK, AR, EES), suggesting that the general relationship between tidal forcing and energy fluxes (Figure 2) also applies to air-water CO_2 exchange.

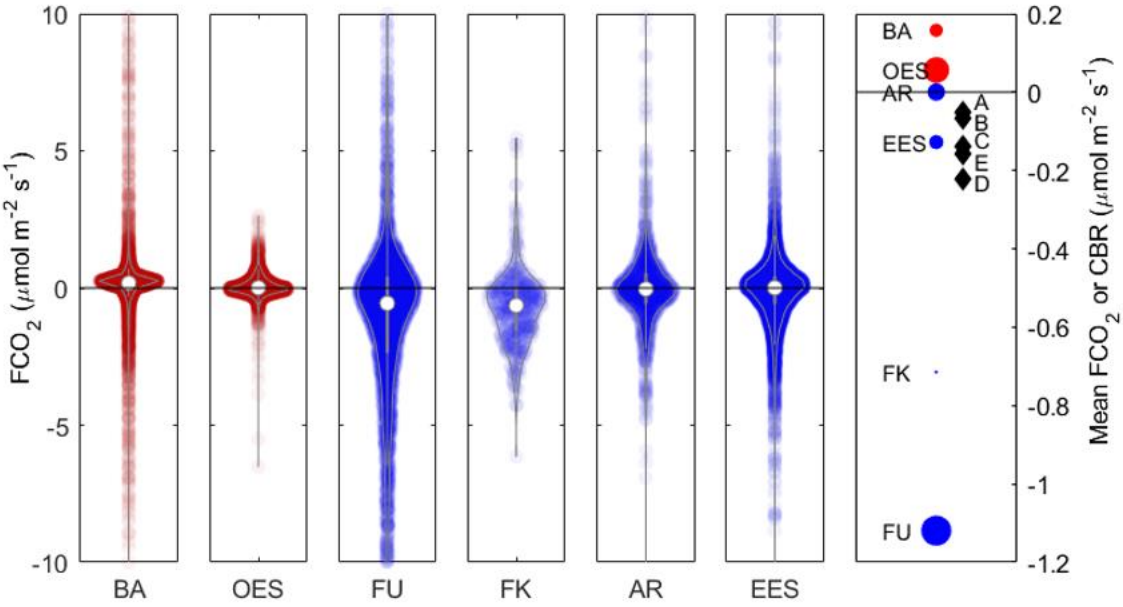

Figure 4. Violin plots of FCO_2 for large-tidal (blue) and small-tidal (red) sites. In the right plot, literature values of carbon burial rates (CBR; black diamonds) are shown alongside average FCO_2 values (blue and red circles), on the same y-axis. The circles are scaled by the number of measurements available for each site. CBR averages are from Samper-Villarreal et al., 2018 (A), Prentice et al., 2020 (B), Duarte et al., 2005 (C), Kennedy et al., 2010 (D), and Sanders et al., 2019 (E).

These average CO_2 evasion/invasion rates are plotted (Figure 4b) alongside organic carbon burial rates (CBR) taken from a global literature review (Samper-Villarreal et al., 2018 [A], Prentice et al., 2020 [B], Duarte et al., 2005 [C], Kennedy et al., 2010 [D], and Sanders et al., 2019 [E]). Converted into the same unit as FCO_2, these literature CBRs ranged from -0.025 to -0.23 µmol C m^{-2} s^{-1}, for a global average of -0.13 ± 0.082 µmol C m^{-2} s^{-1}. The comparison of CBR with FCO_2 should be made with some caution, as CBR represents time scales much longer (decades to centuries) compared with our FCO_2 measurements, for which the longest available dataset is just over three years long.

Nevertheless, for the sites with complete seasonal coverage (BA, EES, FU, OES), it is apt to make a comparison between the rate of carbon storage in sediments and the exchange of CO_2 with the atmosphere. As is evident in Figure 4b, FCO_2 is of similar magnitude to CBR (not always the same direction), indicating that both of these biogeochemical fluxes are relevant to the carbon budget of seagrass meadows. Considering an average CBR of 0.126 µmol m^{-2} s^{-1}, net emissions at BA released CO_2 to the atmosphere at a rate comparable to 125% of mean global organic carbon burial (100% * 0.158/0.126 = 125%). Assuming lateral import and export of DIC and TA were balanced, which is plausible at this site (Van Dam et al., in press), the net effect of this CO_2 emission was to transition the site from a sink for carbon into a small source. It is likely that the relatively high calcification rates in Florida Bay (Howard et al., 2018) are responsible for generating CO_2 in excess of photosynthetic uptake, pushing this site towards net CO_2 emissions. This is a noteworthy finding in light of the commonly-held view that carbonate-rich seagrass

meadows can still be CO_2 sinks due to the import of allochthonous $CaCO_3$ (Saderne et al., 2019). Our finding of net CO_2 emission at BA is the first direct indication that calcification in seagrass meadows can be sufficient to offset autotrophic CO_2 uptake.

Likewise, net CO_2 emissions at OES were 44% of average global CBR. It should be noted that the greater water depth with some wind directions at OES means that water-column processes are likely more important here than at the other sites. At the remaining sites, net negative FCO_2 uptake increased carbon uptake by 888% (FU) and 101% (EES), relative to global average CBR. As discussed later, net CO_2 uptake at these "large-tidal" sites does not necessarily point to increased carbon storage, but rather export of DIC or import of TA to/from adjacent waters. This simple assessment indicates that the consideration of only CBR or FCO_2 alone will bias the magnitude, or even sign (in the case of BA) of the coastal carbon sink. Therefore, we point to a clear need for site-specific measurements of both annually-integrated FCO_2 (by EC, for example) and CBR, which together may significantly increase the reliability of coastal carbon accounting.

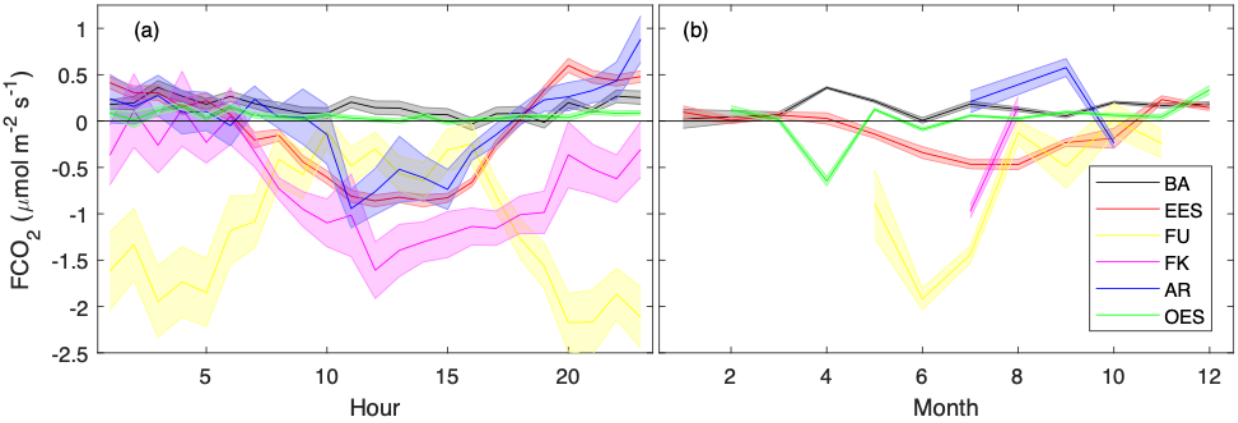

Figure 5. Daily (a) and seasonal (b) climatology of mean FCO_2 for all sites. Negative values of FCO_2 indicate a net CO_2 uptake, while positive values show emission. The shaded areas represent the SE of mean FCO_2 at each hour.

Differences were also evident in the temporal trends in FCO_2 (Figure 5). Some sites exhibited a clear diel cycle of CO_2 uptake (EES, FK, AR) or release (FU) during the day, while other sites were relatively consistent CO_2 sources (BA, OES). A significant global trend of decreasing latent heat flux (LE) with increasing latitude is evident (Figure 6d), which is expected given the similar global trend of decreasing insolation at higher latitude. On the contrary, no relationship was observed between FCO_2 and latitude (Figure 6b). Instead, as suggested by the variation in FCO_2 with tidal setting (Figure 4), and the poor energy balance closure for large-tidal sites (Figure 2), the best predictor for site-averaged FCO_2 was in fact tidal range (Figure 6a).

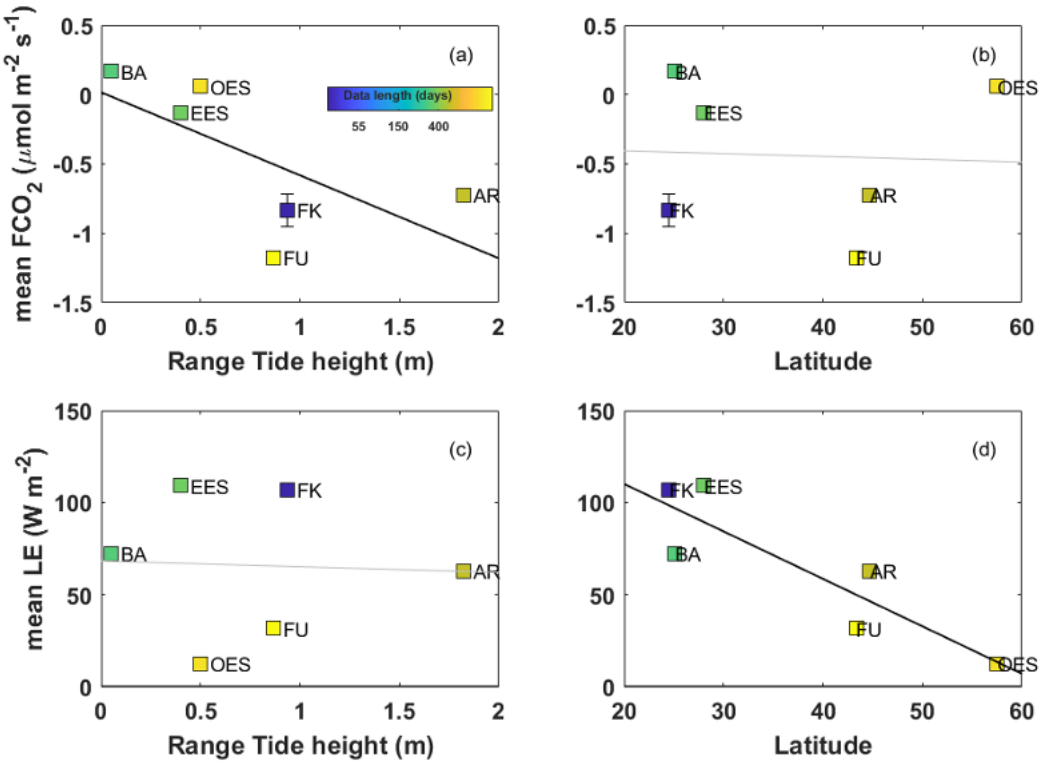

Figure 6. Scatter plots of mean FCO_2 (top panels) and LE (bottom panels) against tidal range and latitude, where the points are colored by the size of the dataset. Linear correlations are shown in bold where slopes are significantly different from zero (b and c; $R^2 = 0.504$,< 0.01 respectively). An estimated mean tidal range at OES of 0.5m (Sahlée et al., 2008) was used for this figure.

3.3. Environmental FCO_2 drivers: Wavelet Coherence

Results from the wavelet coherence analysis are shown in Figure S2, for the following selection of variables: net solar radiation (R_n), water depth (Z_{water}), air temperature (T_{air}), water temperature (T_{water}), wind speed (U_{mean}), and wind direction (U_{dir}). The color indicates the strength of the correlation between each variable and FCO_2 with the phase of this relationship shown by the direction of the arrow. When the variables are in phase (positively correlated), the arrow points right, out of phase (negative correlation) the arrow points left, and when the driver leads FCO_2 by 90^o the arrow points down. Subsequently, these results are summarized in Figure 7, which presents the average R^2 for the entire period of record, collapsed along the x-axis in Fig S2. To prevent times of anti-phase correlation from canceling out in-phase correlations (at the same period), the average presented in Figure 7 was calculated using the absolute value of R^2. As such, Figure 7 only represents the average strength, not the direction, of the correlation between each variable and FCO_2.

3.3.1 Weekly-monthly periods

The importance of each environmental driver on FCO_2 varied across sites and time scales. However, at BA and OES there was generally less power at the daily time scale than there was at weekly-monthly periods. First, as expected for a small-tidal site, Z_{water} was the least predictive

variable in the wavelet coherence analysis at BA, even at the semidiurnal lunar tide (M2 period, ~12.5 hrs). This is in line with the results of the energy budget analysis (Figure 2), supporting the concept that tidal forcing was not an important driver of FCO_2 here. Instead, weekly-monthly scale variations in T_{water}, T_{air}, U_{mean}, U_{dir} were especially prominent as drivers of FCO_2, rivaling the impact of diel R_n variability (Figures 7a, S2). In particular, the strong positive correlation between T_{water} and FCO_2 across multiple time scales supports 1) the role of ecosystem calcification as a putative CO_2 source, and 2) the importance of thermal forcing of air-water gas transfer (Van Dam et al., in review).

As was the case for BA, power at the M2 period was not elevated at OES, indicating that tidal forcing was not an important driver of FCO_2 here. Instead, power was focused at longer weekly-monthly time scales at OES (and BA). Because much of the variability at these longer periods is due to synoptic- or meso-scale events, it seems likely that weather patterns at these intermediate time scales may be important drivers of FCO_2 at both OES and BA. Such weather events have also been shown to enhance methane emissions at OES (Gutiérrez-Loza et al., 2019). Fluxes at OES are also known to exhibit a strong seasonal cycle (Rutgersson et al., 2020), although the presence of data gaps prevented the incorporation of seasonality into this wavelet coherence analysis. The relatively deep water at this site - from less than 5 to greater than 20 m depending on flux footprint – may also support the dominance of long time-scales at OES.

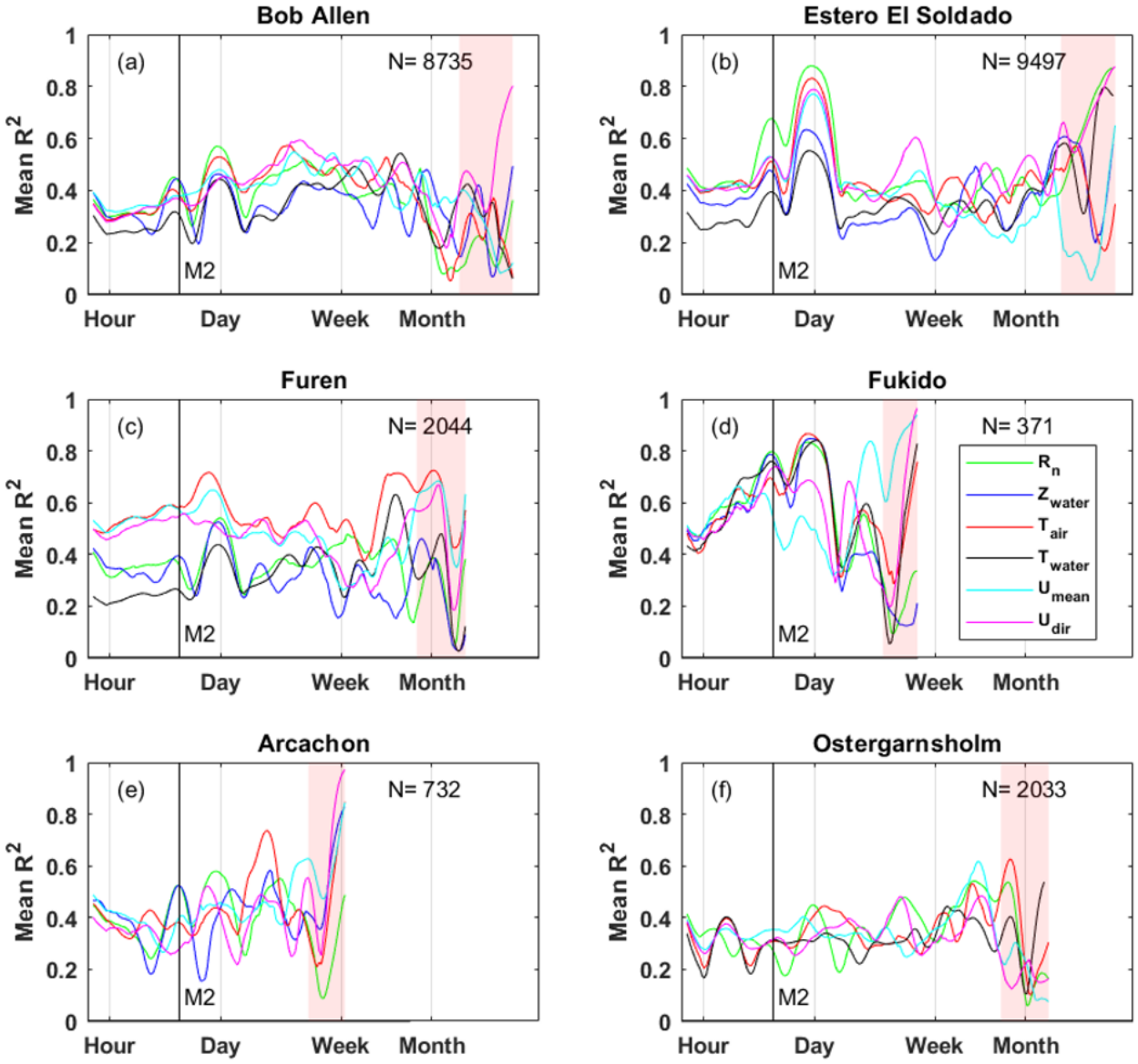

Figure 7. Wavelet coherence analysis summary showing the mean power (R^2) for the relationship between FCO_2 and net solar radiation (R_n), water depth (Z_{water}), air temperature (T_{air}), water temperature (T_{water}), wind speed (U_{mean}), and wind direction (U_{dir}), averaged over the length of each dataset (x-axis in Figure S2). The red shading indicates periods where we suspect uncertainty due to edge effects, estimated as 90% of the maximum period. Because positive and negative R^2 values cancel out when averaged, we calculated this statistic using absolute value R^2. This action effectively sacrifices knowledge of the correlation phase in exchange for a more intuitive summary of the correlation power.

3.3.2 Daily and M2 periods

At both EES and FU, there are clear bands of power at the daily and M2 time scales (Figure S2), supporting the diel trends present in the FCO_2 climatology (Figure 5). At EES, all variables considered are correlated with FCO_2 at the daily time scale, but these variables trade off in

importance over the period of record (Figure S2). For example, U_{mean} is strongly out of phase with FCO_2 during the first half of the study period at EES, while Z_{water} and T_{water} are only weakly correlated with FCO_2. During the second half of the period of record, this trend reverses, with Z_{water} and T_{water} exceeding U_{mean} as drivers of diel variability in FCO_2. Seasonal changes in seagrass productivity at EES is a candidate explanation for these longer-term trends in the drivers of diel-scale variability in FCO_2 and is discussed in detail elsewhere. However, we cannot rule out the importance of seasonal upwelling in the eastern Gulf of California (Lluch-Cota 2000), which may introduce cooler, high-pCO_2 coastal waters to the EES system.

At FU, the diel trend in FCO_2 was opposite of the trend elsewhere, such that CO_2 uptake was greater at night, and decreased during the day (Figure 5). This may appear counterintuitive, given the expectation of greater CO_2 uptake during the day, as supported by photosynthesis-irradiance curves at this site during the summer (Tokoro et al., 2014). However, these estimates of net ecosystem productivity varied from positive to negative over all light regimes in both summer and winter months (Tokoro et al., 2014), indicating that inorganic carbon fluxes were affected by factors other than net ecosystem primary productivity during this time period. Across all periods, T_{air} was the strongest predictor of FCO_2 at the boreal FU site (Figure S2), such that covariations in T_{air} and FCO_2 are in phase (Figure 7c). This in-phase correlation between FCO_2 and T_{air} (and T_{water}), at FU suggests the thermal impact of changing water temperature on pCO_2, where pCO_2 rises during the day as water warms and decreases over night as solubility increases (Takahashi et al., 2002), in line with prior findings at Bob Allen Keys, Florida (Van Dam et al., in review). As with the other large-tidal sites, correlations between Z_{water} and FCO_2 at FU are strongest at the diel and M2 periods, further supporting the role of tidal forcing on air-water CO_2 exchange.

3.3.3 Wavelet coherence: Sites with limited data

Due to the limited length of data for both FK and AR, it was not possible to assess variability at time scales of a week or more. Nevertheless, tidal forcing appeared to play a prominent role at AR, where Z_{water} and FCO_2 were correlated (generally in-phase) at the diel and M2 periods (Figure S2). This is in line with previous findings demonstrating a general trend of CO_2 uptake during low tide and release during high tide at AR (Polsenaere et al., 2012).

At FK, strong anti-phase correlations exist at the diel time scale for R_n, T_{water} and T_{air}, while an in-phase relationship is present between FCO_2 and Z_{water} (Figure S2). The presence of anti-phase relationships between FCO_2 and R_n, T_{water} and T_{air}, strongly suggest photosynthetic CO_2 uptake as a driver of FCO_2 during the short period for which measurements are available at FK. Since CO_2 solubility decreases with increasing temperature, one would expect FCO_2 and air or water temperature to be in phase. The existing anti-phase relationship between these variables suggests that something other than thermal forcing, namely biological CO_2 fixation, caused the daytime CO_2 uptake at FK. The combination of shallow water depths (< 2m) and relatively low phytoplankton Chlorophyll-a (Tokoro et al., 2014) suggests that submerged aquatic vegetation, mostly seagrass, were responsible for the majority of this CO_2 uptake. As with the remaining large-tidal sites, the strong power at the M2 period for most variables (Figure 7d), supports tidal forcing as a key driver of FCO_2.

3.4. Air-side physical drivers of FCO_2

Numerous factors contribute to the physical forcing of gas transfer in shallow coastal waters, including friction with the bottom (Rosentreter et al., 2017; Zappa et al., 2003), water-side convection (Van Dam et al., 2019b, Podgrajsek et al., 2015), breaking waves, biogenic surfactants. Nevertheless, wind speed remains the most commonly-used driver in gas transfer parameterization, even in coastal waters. While a rigorous quantification of gas transfer rates is beyond the scope of this study, our dataset contains valuable information on the turbulent processes responsible for air-sea gas exchange and may help to illustrate features that are globally consistent or variable. Such a comparison is currently absent from the coastal gas-transfer literature.

In the open ocean, the transfer of momentum (and therefore gas) between the sea and air is strongly associated with the wind stress (τ), which is proportional to the atmospheric friction velocity (u_*) through τu^2 (Upstill-Goddard 2006). The shape of the relationship between wind speed and u_*, therefore, is of great interest. When sites are mostly surrounded by water, such that the flux footprint is aquatic across most wind directions (FU, OES), u_* increases linearly with wind speed (U_z), at a slope of approximately 0.035 (Figure 8 c,e). At the remaining sites, which experience a terrestrial influence at certain wind directions (BA, EES, AR), there is a clear dependence of the slope on wind direction (Figure 8 a,b,d). At these sites, when the wind direction is such that the flux footprint is entirely aquatic (blue points for Figure 8 a,b), u_* scales with wind speed at the same 0.035 slope. However, when a terrestrial influence is likely (e.g. winds between 180 to 360^o at BA), the slope between u_* and wind speed increases and becomes variable, as expected for relatively rough terrestrial surfaces. Since a terrestrial influence is not desirable for the present study, we calculated an average ratio of u_*/U_z (0.0924), and discarded FCO_2 values when this ratio was greater than 150% of the mean (i.e. $u_*/U_z > 0.139$). The associated threshold slope of u_*/U_z is shown as the red line in Figure 8.

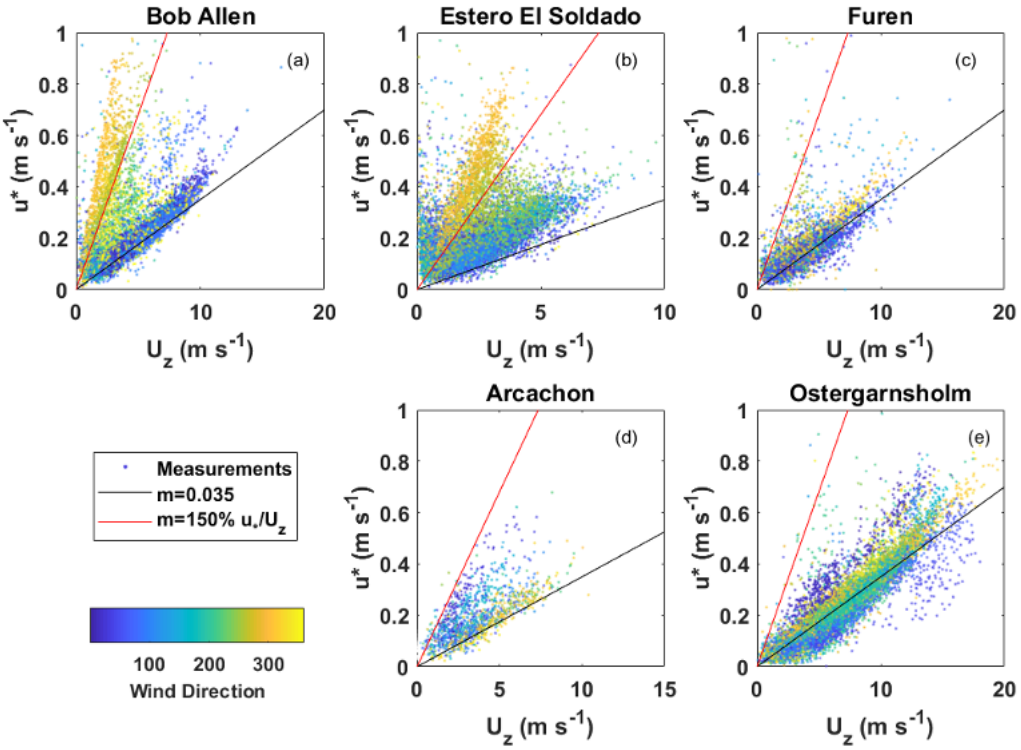

Figure 8. Wind speed at measurement height (U_z) versus friction velocity across sites, colored by wind direction. The black line is a reference slope of 0.035, and the red line shows the slope relating to a u_*/U_z ratio 150% of the average value

The nature of momentum transfer (and thereby gas transfer) can be further assessed through the drag coefficient associated with the measurement height z ($C_{D(z)}$), which is related to the aforementioned ratio of u_*/U_z through $C_{D(z)} =$, where U_z is the wind speed (m s^{-1}) at the measured height. At all sites, calculated values of $C_{D(z)}$ were highly variable with wind speed, but generally exceed parameterizations for the open ocean by a factor of at least 5-10 (Figure 9a). The general distribution of $C_{D(z)}$ with U_z fits the pattern observed in Vickers et al. (2013), who describe three main domains, where 1) $C_{D(z)}$ is large, and not strongly related to U_z (1-4 m s^{-1}), 2) moderate winds (4-10 m s^{-1}) where $C_{D(z)}$ is constant at ~0.01, and 3) a regime of increasing $C_{D(z)}$ at U_z greater than 10 m s^{-1} (only visible for BA and OES in Figure 9b,f).

The elevation in $C_{D(z)}$ above values expected for the open ocean may be related to the increased roughness of immature, 'growing' waves under fetch-limited conditions (Mahrt et al., 1996; Vickers and Mahrt 1997; Rutgersson et al. 2020). Small-scale non-stationary winds have been shown to enhance fluxes above the theoretical expectations for lower wind speeds in marine conditions (Mahrt et al., 2020). This $C_{D(z)}$ enhancement may be related to 'disturbed' or 'growing' wave fields which may be present at low, as well as high, wind speeds (Rutgersson et al., 2020). These 'growing' wave fields, under non-stationary conditions may offer a possible explanation for the observed increase in $C_{D(z)}$ at wind speeds between 1-5 m s^{-1} (Figure 9a).

However, it is clear that other factors may also contribute to this $C_{D(z)}$ enhancement, including bottom-driven turbulence, surfactant activity, shallow water depth (more rapid wave breaking)

and the presence of additional submerged roughness elements (i.e. seagrasses). For example, at very low wind speeds, the combination of increased air-side convection and unstable-to-neutral conditions has been associated with enhanced gas transfer rates (Sahlee et al., 2008; Van Dam et al., in review). However, this effect is not clear in the present dataset, as atmospheric stability (z/L) was not related to these periods of increased $C_{D(z)}$ (not shown).

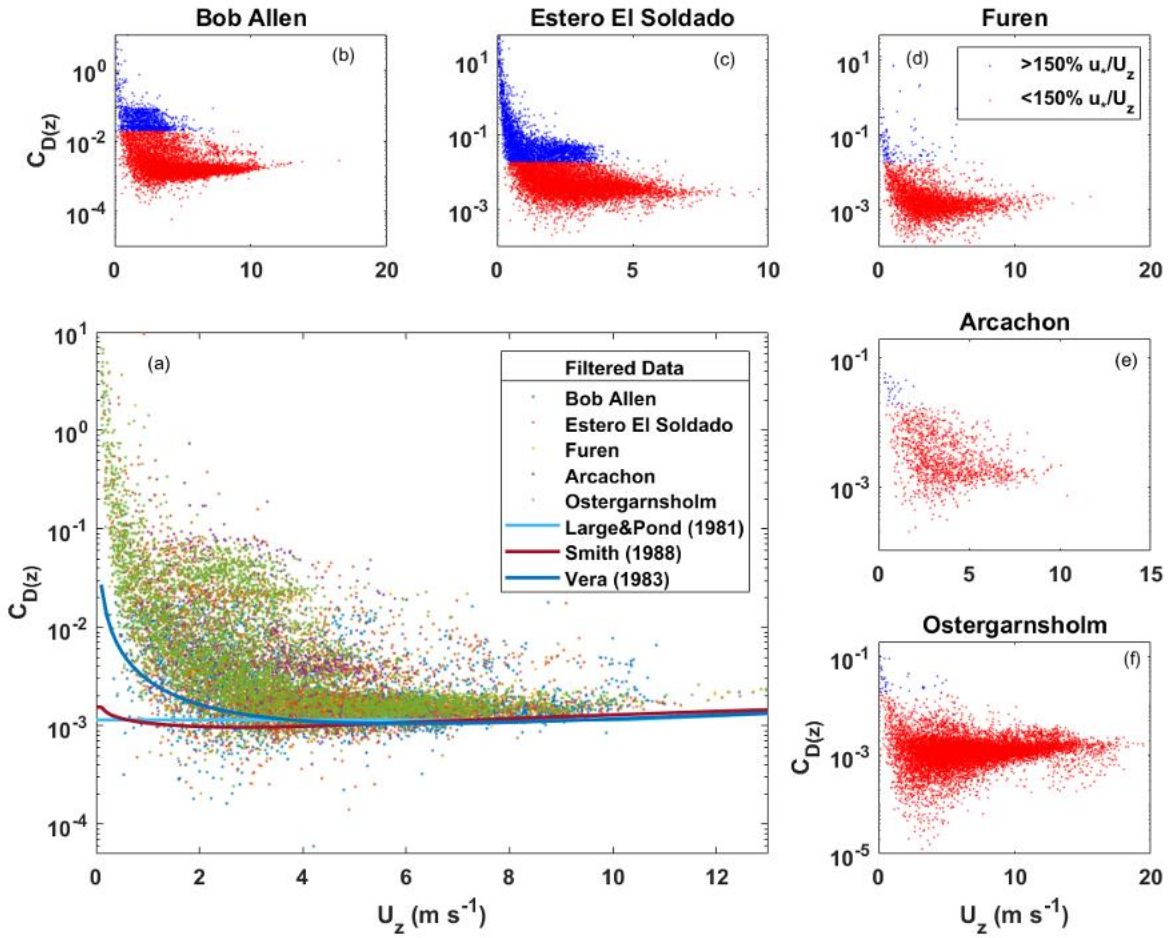

Figure 9. Relationship between U_z and $C_{D(z)}$, after filtering by the u_*/U_z threshold (a). A selection of open-ocean relationships from the literature is depicted in the solid lines. Similar scatterplots for individual sites, showing all data (b-f), including measurements where u_*/U_z exceeded the 150% threshold which are represented by the blue points.

3.5. Global trends

While LE fluxes exhibited a significant latitudinal trend, with net evaporative heat losses increasing towards the equator (Figure 6d), such a trend was not apparent for FCO_2 (Figure 5b). Instead, tidal forcing appears to be a global driver of FCO_2 trends in seagrass meadows, with large-tidal sites exhibiting a greater FCO_2 range (Figure 4), and magnitude toward a CO_2 sink status (Figure 6b), than small-tidal sites. Furthermore, small-tidal sites (BA, OES) responded strongly to variability at time scales longer than a day (Section 3.3.1), while the large-tidal sites (EES, FU, FK) were more sensitive to variability at the M2 and daily time scales (Section 3.3.2).

Many factors may contribute to this global trend in tidal forcing of air-water CO_2 exchange. Tidal currents can enhance rates of gas transfer when bottom-generated turbulence impacts the air-water interface (Ho et al., 2014; Rosentreter et al., 2017; Upstill-Goddard 2006), but under certain conditions may suppress gas transfer when currents are strong enough to re-suspend sediments (Abril et al., 2009). Similarly, tidal impacts on sediment biogeochemical cycling can cause variations in the air-water CO_2 gradient. Sediment resuspension and tidal oxygen pumping can enhance rates of aerobic respiration enhancing CO_2 release (Almroth-Rosell, et al., 2012; Ståhlberg et al., 2006). Elsewhere, current can generate pressure gradients which flush anaerobic respiration products from sediments, either increasing or decreasing pCO_2 in proportion to DIC and alkalinity fluxes (Santos et al., 2015). At a larger scale, tidal mixing drives inorganic carbon "outwelling" from coastal marshes (Cai et al., 1999), with an effect on air-water CO_2 exchange that should be proportional to the DIC:TA export ratio. Because these factors act synchronously, it is impossible to attribute the global trend of decreasing magnitude and range in FCO_2 with a single 'tidal' factor. Nevertheless, it is clear that tidal dynamics must be considered when the net carbon sink/source status of seagrass meadows is assessed.

4. Summary and conclusion

We produced a global synthesis of all available eddy covariance measurements of air-water CO_2 exchange (FCO_2) over shallow, seagrass-dominated environments. At most sites, the absolute magnitude of FCO_2 was as large or larger than published "blue carbon" burial rates (CBR). Elsewhere, CO_2 fluxes in excess of organic carbon storage have been reported for Japanese seagrasses (Kuwae and Hori 2019), but the present study demonstrates that this is a global, not regional phenomenon. At seagrass meadows functioning as net sources of CO_2 to the atmosphere (BA, OES), FCO_2 was between 44 (OES) -115 (BA)% of global average CBR (0.13 µmol m^{-2} s^{-1}). Assuming minimal lateral exchange, this effectively converted BA from a net carbon sink into a net carbon source. Datasets for both BA and OES contain substantial and representative measurements during all seasons (Figure 5b), indicating that while there is substantial seasonal variability (Rutgersson et al., 2020) in FCO_2, these sites are indeed both net sources of CO_2 to the atmosphere. We suggest net ecosystem calcification as a putative source of this CO_2, due to the correlation between FCO_2 and temperature, and the large $CaCO_3$ stocks present at this site (Howard et al., 2018). For the remaining sites, net CO_2 uptake was ~100% (EES) to over 800% (FU) of global average CBR. However, additional seasonal measurements would improve the reliability of this assessment.

We then identified drivers of FCO_2 that are present across the large range in seagrass ecosystems, which are responsible for generating this 'disagreement' between CBR and net carbon sink/source status. First, we considered the leverage exerted on FCO_2 by the physical processes affecting rates of air-water CO_2 exchange, and found that surface roughness ($C_{D(z)}$) was always greater than expected for the open ocean, suggesting a near-universals enhancement of gas transfer in shallow, coastal waters. Next, many lines of evidence point to tidal-driven exchanges as a key driver for FCO_2 over seagrass meadows. First, we show a clear relationship between tidal range and energy balance residual, which persists across our global range in study sites. This energy balance 'leakage' under tidal conditions indicates that the lateral exchange of

dissolved CO_2 (and organic carbon) is a major factor contributing to the observed mismatch between FCO_2 and CBR. The negative relationship between average tidal range and FCO_2 (Figure 6) provides further evidence that the sites acting as net CO_2 sinks may have done so in response to tidal forcing. Lastly, the results of our wavelet coherence analysis support the role of tidal forcing on FCO_2, given the increase in power at the M2 period, especially for EES, AR, and FU (Figure 9b,c,e).

In conclusion, we report high rates of air-water CO_2 exchange over seagrass meadows, which may significantly alter the net carbon storage capacity of these 'blue carbon' ecosystems. This study argues the need for a more comprehensive approach to future 'blue carbon' assessments, which should consider organic carbon storage in the context of other carbon fluxes, including air-water CO_2 exchange. Future studies can build on this work by investigating the role of tidal and thermal forcing, which may affect CO_2 fluxes by enhancing (or suppressing) the turbulence responsible for air-water gas exchange, but may also transport excess CO_2 away from or to seagrass meadows. And, while the present study was limited to CO_2, many of the factors affecting air-sea CO_2 transfer are also apply to other greenhouse gases including CH_4 and N_2O. There is also a clear need for direct CO_2 flux measurements in the southern hemisphere, of which none are presently available.

Acknowledgments

This work was primarily supported by the DAAD grant #57429828, from funds of the German Federal Ministry of Education and Research (BMBF). This work was supported by the US National Science Foundation through the Florida Coastal Everglades Long-Term Ecological Research program under Grants No. DEB-1237517 and DEB-1832229. We thank Prof Dr Helmuth Thomas and Dr Mary Zeller for their feedback on this manuscript, which significantly improved its quality. Technical staff at LI-COR were also indispensable, and we specifically thank Israel Begashaw and James Kathilankal for their patience and support. We also appreciate the assistance of the National Parks Service, who allowed equipment to be deployed in the Everglades National Park at Bob Allen Keys, under Permit [EVER-2018-SCI-0072]. Measurements at Estero El Soldado were possible with funds from the Mexican National Council of Science and Technology (CONACYT) grant # 278608 and assistance of the Ecology Commission from Sonora (CEDES). This is contribution #[updated upon publication] from the Coastlines and Oceans Division in The Institute of Environment at Florida International University. TK and TT was funded in part by Grants-in-Aid for Scientific Research (KAKENHI) grant numbers JP18H04156 from the Japan Society for the Promotion of Science. The Östergarnsholm site is a part of the ICOS (Integrated Carbon Observation Study) and funded by Swedish Research Council and Uppsala University. Technical staff working at the Östergarnsholm station are greatly acknowledged. The Arcachon study was supported by the ANR project PROTIDAL and the Aquitaine region; we are grateful to all our colleagues from the University of Bordeaux and INRA Bordeaux who participated to EC field deployments, data analysis and associated constructive reflexions.

Data Availability Statement

Data are published openly at doi 10.6084/m9.figshare.12161478 for BA, and 10.5281/zenodo.3372787 for EES. The remaining datasets for FU, FK, AR, and OES are available under previous publications Tokoro et al. (2014), Polsenaere et al. (2012), and Rutgersson et al. (2020).

Competing Interests

The authors declare no conflicts of interest

References

Abril, G., Commarieu, M. V., Sottolichio, A., Bretel, P., & Guérin, F. (2009). Turbidity limits gas exchange in a large macrotidal estuary. *Estuarine, Coastal and Shelf Science*, *83*(3), 342–348. https://doi.org/10.1016/j.ecss.2009.03.006

Almroth-Rosell, E., Tengberg, A., Andersson, S., Apler, A., & Hall, P. O. J. J. (2012). Effects of simulated natural and massive resuspension on benthic oxygen, nutrient and dissolved inorganic carbon fluxes in Loch Creran, Scotland. *Journal of Sea Research*, *72*, 38–48. https://doi.org/10.1016/j.seares.2012.04.012

Al-Haj, A. N., & Fulweiler, R. W. (2020). A synthesis of methane emissions from shallow vegetated coastal ecosystems. Global Change Biology, 26(5), 2988–3005. https://doi.org/10.1111/gcb.15046

Armitage, A. R., Frankovich, T. A., & Fourqurean, J. W. (2011). Long-Term Effects of Adding Nutrients to an Oligotrophic Coastal Environment. *Ecosystems*, *14*(3), 430–444. https://doi.org/10.1007/s10021-011-9421-2

Aubinet, M., Grelle, A., Ibrom, A., Rannik, U., Moncrieff, J., Foken, T., Kowalski, A. S., Martin, P. H., Berbigier, P., Bernhofer, C. H., Clement, R., Elbers, J., Granier, A., Grunwald, T., Mor- genstern, K., Pilegaard, K., Rebmann, C., Snijders, W., Valentini, R., and Vesala, T.: Estimates of the annual net carbon and water exchange of European forests: the EUROFLUX methodology, Adv. Ecol. Res., 30, 113–175, 2000.

Barreras-Apodaca, A. & Sánchez-Mejía, Z.M. (2019). Eddy Covariance observations of three different sites from Estero El Soldado, Sonora, Mexico, doi:10.5281/zenodo.3372787

Benítez-Valenzuela, L. I., & Sanchez-Mejia, Z. M. (2020). Observations of turbulent heat fluxes variability in a semiarid coastal lagoon (Gulf Of California). Atmosphere, 11(6), 15–17. https://doi.org/10.3390/atmos11060626

Berg, P., Delgard, M. L., Polsenaere, P., Mcglathery, K. J., Doney, S. C., & Berger, A. C. (2019). Dynamics of benthic metabolism, O2 ,and pCO2 in a temperate seagrass meadow. *Limnology and Oceanography*, 1–19. https://doi.org/10.1002/lno.11236.

Burba, G. (2010). *Eddy Covariance Method for Scientific, Industrial, Agricultural, and Regulatory Applications*. LI-COR Biosciences, Lincoln, Nebraska. ISBN: 978-0-615-76827-4

610 Burdige, D. J., & Zimmerman, R. C. (2002). Impact of Sea Grass Density on Carbonate
611 Dissolution in Bahamian Sediments Impact of sea grass density on carbonate dissolution in
612 Bahamian sediments. *Limnology and Oceanography*, *47*, 1751–1763.
613 https://doi.org/10.4319/lo.2002.47.6.1751

614 Burdige, D. J., Hu, X., & Zimmerman, R. C. (2010). The widespread occurrence of coupled
615 carbonate dissolution/reprecipitation in surface sediments on the Bahamas Bank. *American*
616 *Journal of Science*, *310*(6), 492–521. https://doi.org/10.2475/06.2010.03

617 Carmen B, Krause-Jensen D, Alcoverro T, Marbà N, Duarte CM, van Katwijk MM, Pérez M,
618 Romero J, Sánchez-Lizaso JL, Roca G, Jankowska E, Pérez-Lloréns JL, Fournier J,
619 Montefalcone M, Pergent G, Ruiz JM, Cabaço S, Cook K, Wilkes RJ, Moy FE, Trayter
620 GMR, Arañó XS, de Jong DJ, Fernández-Torquemada Y, Auby I, Vergara JJ, Santos R.
621 2019. Recent trend reversal for declining European seagrass meadows. Nature
622 Communications 10:3356.

623 Cai, W.-J., Pomeroy, L. R., Moran, M. A., & Wang, Y. (1999). Oxygen and carbon dioxide mass
624 balance for the estuarine-intertidal marsh complex of five rivers in the Southeastern U.S.
625 *Limnology and Oceanography*, *44*(3), 639–649. https://doi.org/10.4319/lo.1999.44.3.0639

626 Dürr, H. H., Laruelle, G. G., van Kempen, C. M., Slomp, C. P., Meybeck, M., & Middelkoop, H. (2011).
627 Worldwide typology of nearshore coastal systems: Defining the estuarine filter of river inputs to the
628 oceans. Estuaries and Coasts, 34(3), 441–458. https://doi.org/10.1007/ s12237-011-9381-y

629 Dollar, S. J., Smith, S. V., Vink, S. M., Obrebski, S., & Hollibaugh, J. T. (1991). Annual cycle of
630 benthic nutrient fluxes in Tomales Bay, California, and contribution of the benthos to total
631 ecosystem metabolism. *Marine Ecology Progress Series*, *79*(1–2), 115–125.
632 https://doi.org/10.3354/meps079115

633 Duarte, C. M., Middelburg, J. J., & Caraco, N. (2005). Major role of marine vegetation on the
634 oceanic carbon cycle. *Biogeosciences*, *2*, 1–8. https://doi.org/10.5194/bg-2-1-2005

635 Duarte, C. M., Marbà, N., Gacia, E., Fourqurean, J. W., Beggins, J., Barrón, C., & Apostolaki, E.
636 T. (2010). Seagrass community metabolism: Assessing the carbon sink capacity of seagrass
637 meadows. *Global Biogeochemical Cycles*, *24*(4), 1–8.
638 https://doi.org/10.1029/2010GB003793

639 Eyre, B. D., & Ferguson, A. J. P. (2002). Comparison of carbon production and decomposition,
640 benthic nutrient fluxes and denitrification in seagrass, phytoplankton, benthic microalgae-
641 and macroalgae-dominated warm-temperate Australian lagoons. *Marine Ecology Progress*
642 *Series*, *229*, 43–59. https://doi.org/10.3354/meps229043

643 Fennel, K., Alin, S., Wang, Z. A., Barbero, L., Shadwick, E., Cooley, S., … Hernandez-Ayon, J.
644 M. (2019). Carbon cycling in the North American coastal ocean: A synthesis.
645 *Biogeosciences Discussions*, *16*, 1281–1304. https://doi.org/10.5194/bg-2018-420

Fourqurean, J. W., Duarte, C. M., Kennedy, H., Marbà, N., Holmer, M., Mateo, M. A., … Serrano, O. (2012). Seagrass ecosystems as a globally significant carbon stock. *Nature Geoscience*, *5*(7), 505–509. https://doi.org/10.1038/ngeo1477

Friedlingstein, P., Jones, M. W., O'Sullivan, M., Andrew, R. M., Hauck, J., Peters, G. P., … Zaehle, S. (2019). Global carbon budget 2019. *Earth System Science Data*, *11*(4), 1783–1838. https://doi.org/10.5194/essd-11-1783-2019

Gazeau, F., Borges, A. V., Barrón, C., Duarte, C. M., Iversen, N., Middelburg, J. J., … Gattuso, J. P. (2005). Net ecosystem metabolism in a micro-tidal estuary (Randers Fjord, Denmark): Evaluation of methods. *Marine Ecology Progress Series*, *301*, 23–41. https://doi.org/10.3354/meps301023

Grinsted, A., Moore, J.C., Jevrejeva, S., 2004. Application of the cross wavelet transform and wavelet coherence to geophysical time series. Nonlinear processes in geophysics 11, 561-566.

Gutiérrez-Loza, L., Wallin, M. B., Sahlée, E., Nilsson, E., Bange, H. W., Kock, A., & Rutgersson, A. (2020). Measurement of Air-Sea Methane Fluxes in the Baltic Sea Using the Eddy Covariance Method. *Frontiers in Earth Science*, *7*(May), 1–13. https://doi.org/10.3389/feart.2019.00093

Ho, D. T., Ferrón, S., Engel, V. C., Larsen, L. G., & Barr, J. G. (2014). Air-water gas exchange and CO 2 flux in a mangrove-dominated estuary. *Geophysical Research Letters*, *41*(1), 108–113. https://doi.org/10.1002/2013GL058785

Howard, J. L., Creed, J. C., Aguiar, M. V. P., & Fouqurean, J. W. (2018). CO2 released by carbonate sediment production in some coastal areas may offset the benefits of seagrass "Blue Carbon" storage. *Limnology and Oceanography*, *63*(1), 160–172. https://doi.org/10.1002/lno.10621

Hu, X., & Burdige, D. J. (2007). Enriched stable carbon isotopes in the pore waters of carbonate sediments dominated by seagrasses: Evidence for coupled carbonate dissolution and reprecipitation. *Geochimica et Cosmochimica Acta*, *71*(1), 129–144. https://doi.org/10.1016/j.gca.2006.08.043

Kennedy, H., Beggins, J., Duarte, C. M., Fourqurean, J. W., Holmer, M., Marbá, N., & Middelburg, J. J. (2010). Seagrass sediments as a global carbon sink: Isotopic constraints. *Global Biogeochemical Cycles*, *24*(4), 1–8. https://doi.org/10.1029/2010GB003848

Kuwae, T., & Hori, M. (2019). Blue Carbon in Shallow Coastal Ecosystems. In *Blue Carbon in Shallow Coastal Ecosystems*. https://doi.org/10.1007/978-981-13-1295-3

Laruelle, G. G., Cai, W. J., Hu, X., Gruber, N., Mackenzie, F. T., & Regnier, P. (2018). Continental shelves as a variable but increasing global sink for atmospheric carbon dioxide. *Nature Communications*, *9*(1), 1–11. https://doi.org/10.1038/s41467-017-02738-z

Legge, O., , Martin Johnson , Natalie Hicks , Tim Jickells , Markus Diesing , John Aldridge, J., Andrews , Yuri Artioli , Dorothee C. E. Bakker , Michael T. Burrows , Nealy Carr, G. C.,

682 Stacey Felgate , Liam Fernand , Naomi Greenwood , Sue Hartman , Silke Kröger, G. L.,
683 Claire Mahaffey , Daniel J Mayor , Ruth Parker , Ana M Queirós , Jamie D. Shutler, T. S.,
684 Henrik Stahl , Jonathan Tinker , Graham J.C. Underwood , Johan van der Molen, S. W., &
685 Keith Weston, P. W. (2020). Carbon on the Northwest European Shelf: Contemporary
686 Budget and Future Influences. *Frontiers in Marine Science Specialty*, *7*(March).
687 https://doi.org/10.3389/fmars.2020.00143

688 Long, M., Berg, P., & Falter, J. (2015). Seagrass metabolism across a productivity gradient using
689 the eddy covariance, Eulerian control volume, and biomass addition techniques. *Journal of*
690 *Geophysical Research: Oceans*, *120*, 2676–2700. https://doi.org/10.1002/2014JC010441

691 Long, M., Berg, P., & Falter, J. (2015). Seagrass metabolism across a productivity gradient using
692 the eddy covariance, Eulerian control volume, and biomass addition techniques. *Journal of*
693 *Geophysical Research: Oceans*, *120*, 2676–2700. https://doi.org/10.1002/2014JC010441

694 Lluch-Cota, S.-E. (2000). Coastal upwelling in the eastern Gulf of California. *Oceanologica*
695 *Acta*, *23*, 731–740.

696 Macreadie, P. I., Serrano, O., Maher, D. T., Duarte, C. M., & Beardall, J. (2017). Addressing
697 calcium carbonate cycling in blue carbon accounting. *Limnology and Oceanography*
698 *Letters*, (Tyrrell 2008), 195–201. https://doi.org/10.1002/lol2.10052

699 Macreadie, P. I., Et. al. (2019). The future of Blue Carbon science. *Nature Communications*, 1–
700 13. https://doi.org/10.1038/s41467-019-11693-w

701 Mahrt, L., Vickers, D., Howell, J., Højstrup, J., Wilczak, J. M., Edson, J., & Hare, J. (1996). Sea
702 surface drag coefficients in the Risø Air Sea Experiment. *Journal of Geophysical Research*
703 *C: Oceans*, *101*(C6), 14327–14335. https://doi.org/10.1029/96JC00748

704 Mahrt, L., E. Nilsson, H. Pettersson and A. Rutgersson (2020) Sea-surface stress driven by
705 small-scale non-stationary winds. Bound. Layer Met., https://doi.org/10.1007/s10546-020-
706 00518-9

707 Oreska, M. P. J., McGlathery, K. J., Aoki, L. R., Berger, A. C., Berg, P., & Mullins, L. (2020). The
708 greenhouse gas offset potential from seagrass restoration. Scientific Reports, 10(1), 1–15.
709 https://doi.org/10.1038/s41598-020-64094-1

710 Perez, D. I., Phinn, S. R., Roelfsema, C. M., Shaw, E., Johnston, L., & Iguel, J. (2018). Primary
711 Production and Calcification Rates of Algae-Dominated Reef Flat and Seagrass Communities.
712 *Journal of Geophysical Research: Biogeosciences*, *123*(8), 2362–2375.
713 https://doi.org/10.1029/2017JG004241

714 Plus M., Dalloyau S., Trut G., Auby I.., De Montaudouin X., Emery É., Noël C., Viala C. (2010).
715 Long-term evolution (1988–2008) of *Zostera* spp. meadows in Arcachon Bay (Bay of
716 Biscay). *Estuarine, Coastal and Shelf Science*, *87*(2), 357-366.

717 Podgrajsek, Sahlée, and Rutgersson (2015), Diel cycle of lake-air CO_2 flux from a shallow lake
718 and the impact of waterside convection on the transfer velocity, *J. Geophys. Res.*
719 *Biogeosciences*, doi:10.1002/2014JG002781.

720 Polsenaere, P., Lamaud, E., Lafon, V., Loustau, D., Delille, B., Deborde, J., … Abril, G. (2012).
721 Spatial and temporal CO2 exchanges measured by Eddy Covariance over a temperate
722 intertidal flat and their relationships to net ecosystem production. *Biogeosciences*, *9*(1),
723 249–268. https://doi.org/10.5194/bg-9-249-2012

724 Prentice, C., Poppe, K. L., Lutz, M., Murray, E., Stephens, T. A., Spooner, A., … Klinger, T.
725 (2020). A Synthesis of Blue Carbon Stocks, Sources, and Accumulation Rates in Eelgrass
726 (Zostera marina) Meadows in the Northeast Pacific. *Global Biogeochemical Cycles*, *34*(2),
727 1–16. https://doi.org/10.1029/2019gb006345

728 Röhr, M. E., Holmer, M., Baum, J. K., Björk, M., Chin, D., Chalifour, L., … Deyanova, D.
729 (2018). Blue Carbon Storage Capacity of Temperate Eelgrass (Zostera marina) Meadows.
730 *Global Biochemical Cycles*, 1457–1475. https://doi.org/10.1029/2018GB005941

731 Rosentreter, J. A., Maher, D. T., Ho, D. T., Call, M., Barr, J. G., & Eyre, B. D. (2017). Spatial
732 and temporal variability of CO2 and CH4 gas transfer velocities and quantification of the
733 CH4 microbubble flux in mangrove dominated estuaries. *Limnology and Oceanography*,
734 *62*(2), 562–578. https://doi.org/10.1002/lno.10444

735 Rutgersson, A., Heidi Pettersson, Erik Nilsson, Hans Bergström, Marcus B.E. Wallin, E.
736 Douglas Nilsson, Erik Sahlée, Lichuan E. Wu & E. Monica Mårtensson (2020) Using land-
737 based stations for air–sea interaction studies, Tellus A: Dynamic Meteorology and
738 Oceanography, 72:1, 1-23, DOI: 10.1080/16000870.2019.1697601

739 Saderne, V., Geraldi, N. R., Macreadie, P. I., Maher, D. T., Middelburg, J. J., Serrano, O., …
740 Duarte, C. M. (2019). Role of carbonate burial in Blue Carbon budgets. *Nature*
741 *Communications*, *10*. https://doi.org/10.1038/s41467-019-08842-6

742 Sahlée, E., Smedman, A.-S., Högström, U., & Rutgersson, A. (2008). Reevaluation of the Bulk
743 Exchange Coefficient for Humidity at Sea during Unstable and Neutral Conditions. *Journal*
744 *of Physical Oceanography*, *38*(1), 257–272. https://doi.org/10.1175/2007jpo3754.1

745 Samper-Villarreal, J., Mumby, P. J., Saunders, M. I., Barry, L. A., Zawadzki, A., Heijnis,
746 H., Morelli, G., & Lovelock, C. E. (2018). Vertical accretion and carbon burial rates in
747 subtropical seagrass meadows increased following anthropogenic pressure from European
748 colonisation. *Estuarine Coastal and Shelf Science*, **202**, 40– 53.

749 Sanders, C. J., Maher, D. T., Smoak, J. M., & Eyre, B. D. (2019). Large variability in organic
750 carbon and CaCO3 burial in seagrass meadows: A case study from three Australian
751 estuaries. *Marine Ecology Progress Series*, *616*, 211–218.
752 https://doi.org/10.3354/meps12955

753 Santos, I. R., Beck, M., Brumsack, H.-J. J., Maher, D. T., Dittmar, T., Waska, H., & Schnetger,
754 B. (2015). Porewater exchange as a driver of carbon dynamics across a terrestrial-marine
755 transect: Insights from coupled 222Rn and pCO2 observations in the German Wadden Sea.
756 *Marine Chemistry*, *171*, 10–20. https://doi.org/10.1016/j.marchem.2015.02.005

757 Ståhlberg, C., Bastviken, D., Svensson, B. H., & Rahm, L. (2006). Mineralisation of organic
758 matter in coastal sediments at different frequency and duration of resuspension. *Estuarine,*
759 *Coastal and Shelf Science*, *70*(1–2), 317–325. https://doi.org/10.1016/j.ecss.2006.06.022

760 Takahashi, T., Sutherland, S. C., Sweeney, C., Poisson, A., Metzl, N., Tilbrook, B., … Nojiri, Y.
761 (2002). Global sea – air CO2 flux based on climatological surface ocean pCO2 , and
762 seasonal biological and temperature effects. *Deep Sea Research Part II: Topical Studies in*
763 *Oceanography*, *49*(9–10), 1601–1622. https://doi.org/10.1016/S0967-0645(02)00003-6

764 Tokoro, T., Hosokawa, S., Miyoshi, E., Tada, K., Watanabe, K., Montani, S., … Kuwae, T. (2014). Net
765 uptake of atmospheric CO2 by coastal submerged aquatic vegetation. *Global Change Biology*,
766 *20*(6), 1873–1884. https://doi.org/10.1111/gcb.12543

767 Tokoro, T., & Kuwae, T. (2018). *Improved Post-processing of Eddy-Covariance Data to*
768 *Quantify Atmosphere – Aquatic Ecosystem CO2 Exchanges*. *5*(August), 1–11.
769 https://doi.org/10.3389/fmars.2018.00286

770 Torrence, C., Compo, G.P., 1998. A practical guide to wavelet analysis. Bulletin of the American
771 Meteorological society 79, 61-78.

772 Upstill-Goddard, R. C. (2006). Air–sea gas exchange in the coastal zone. *Estuarine, Coastal and*
773 *Shelf Science*, *70*(3), 388–404. https://doi.org/10.1016/j.ecss.2006.05.043

774 Vickers, D., Mahrt, L. (1997). Fetch Limited Drag Coefficients. *Boundary-Layer*
775 *Meteorology* **85,** 53–79. https://doi.org/10.1023/A:1000472623187

776 Vickers, D., Mahrt, L., & Andreas, E. L. (2013). Estimates of the 10-m Neutral Sea Surface Drag
777 Coefficient from Aircraft Eddy-Covariance Measurements. *Journal of Physical*
778 *Oceanography*, *43*(2), 301–310. https://doi.org/10.1175/JPO-D-12-0101.1

779 Van Dam, B. R., Lopes, C., Osburn, C. L., & Fourqurean, J. W. (2019a). Net heterotrophy and
780 carbonate dissolution in two subtropical seagrass meadows. *Biogeosciences*, *16*, 4411–
781 4428. https://doi.org/10.5194/bg-2019-191

782 Van Dam, B. R., Edson, J. B., & Tobias, C. (2019b). Parameterizing Air-Water Gas Exchange in
783 the Shallow, Microtidal New River Estuary. *Journal of Geophysical Research:*
784 *Biogeosciences*, 2018JG004908. https://doi.org/10.1029/2018JG004908

785 Zappa, C. J., Raymond, P. A., Terray, E. A., & Mcgillis, W. R. (2003). Variation in Surface
786 Turbulence and the Gas Transfer Velocity in a Macro-Tidal Estuary. *Estuaries*, *26*(6),
787 1401–1415.